

Contents lists available at ScienceDirect

Journal of Crystal Growth

journal homepage: www.elsevier.com/locate/jcrysgro





Effect of heat transfer on the growth angles observed in meniscus-defined solidification

Nojan Bagheri-Sadeghi, Brian T. Helenbrook *

Department of Mechanical & Aerospace Engineering, Clarkson University, Potsdam, NY 13699-5725, United States

ARTICLE INFO

Communicated by T. Duffar

Kevwords:

A1 Heat transfer

A1 Interfaces

A1 Solidification

A1 Triple-phase line

A2 Growth from melt

A2 Horizontal ribbon growth

ABSTRACT

The interfacial geometry at the triple-phase line is defined by the growth angle, θ_{gr} , and the solid angle, θ_s , θ_{gr} is the angle between the melt-gas interface and the plane defined by the solid-gas interface, and θ_s is the angle between the solid-melt and solid-gas interfaces. A local analysis of the temperature field near the triple-phase line of solidification was used to identify the interfacial configurations that have a nonsingular heat flux. It was shown that there is a nonsingular region in the θ_s - θ_{gr} plane, the bounds of which depend on ratios of thermal conductivities. Results indicate that experimentally observed growth angles seem to fall into the nonsingular regions although experimental data is highly limited. Predictions of growth angles based on interfacial tensions were also examined but it was difficult to determine if either criterion was predictive.

1. Introduction

An important characteristic of meniscus-defined solidification processes from the melt, such as Czochralski, floating-zone or horizontal ribbon growth (HRG), is the triple-phase line where the melt, crystal, and the inert phase (often a gas) meet. Understanding the physics of the triple-phase line is crucial for achieving stable and steady crystal growth in these processes [1–13]. The geometry near the triple-phase line can be defined by the solid angle, θ_s , and the growth angle θ_{gr} . The growth angle is the angle between the direction of motion of the triple-phase line and the tangent to the liquid–gas interface. 1 Fig. 1a shows a schematic of the triple-phase line designated as $\rm O_{TPL}$ with velocity relative to the solid of V_{TPL} where the interfacial curvatures near the triple-phase line are assumed to be small.

One phenomenon that is poorly understood at the triple-phase line is the growth angle. Its value is often associated with a condition derived from the minimization of interfacial energies at the triple-phase line [1,4], although there is little experimental evidence that this is predictive. The condition of minimization of interfacial energies at the triple-phase line reduces to the equilibrium of interfacial tensions and a balance of moments due to the variation of these tension forces with curvature at the triple-phase line [1,4]. For liquid–gas interfaces, the magnitude of the surface tension vector is the same as the interfacial energy. However, they are different for solid-melt and solid–gas interfaces as the interfacial energy is based on reversible work of creation

of the interface without any elastic or plastic deformation whereas surface tension also includes stresses due to such solid deformations (see section 1.1.3 of [1] for more details). For this discussion, this subtlety is neglected.

For small interfacial curvatures at the triple-phase line the moment terms can be neglected [4]. Although, Voronkov [1,14] argues that for faceted interfaces where there is a high level of supercooling, the curvature of solid interfaces near the triple-phase line can be large leading to a significant difference between observed and actual growth angles at the triple-phase line. We are unaware of any experimental confirmation of this, however, so in the following interfacial curvatures are neglected. Therefore, the condition reduces to the balance of interfacial tensions only. Fig. 1b shows the balance of interfacial tensions where σ_{sg} , σ_{lg} , and σ_{sl} denote the interfacial energies of solid– gas, melt-gas, and solid-liquid interfaces respectively. Considering the equilibrium for a circular section at a small distance r about the triplephase line, the surface stresses on the circular perimeter for each of the three phases should be considered in addition to these interfacial tensions. It is reasonable to assume that the equilibrium reduces to the balance of interfacial tensions as the surface areas corresponding to the stresses approach zero as the radius of the circular section goes to zero.

The values of θ_{gr} are measured for a number of materials and summarized by Eustathopoulos et al. [1]. However, in most cases, the corresponding θ_s is not reported. So, even assuming small local

^{*} Corresponding author.

E-mail address: bhelenbr@clarkson.edu (B.T. Helenbrook).

¹ Equivalently, growth angle can be defined as the angle between the solid–gas and melt-gas interface planes at the triple-phase line. The growth angle condition defines the growth direction of the triple-phase line during solidification. However, this condition does not apply to a melting or non-solidifying solid [1,2] (back-melting can happen in unsteady HRG as shown in Ref. [3]).

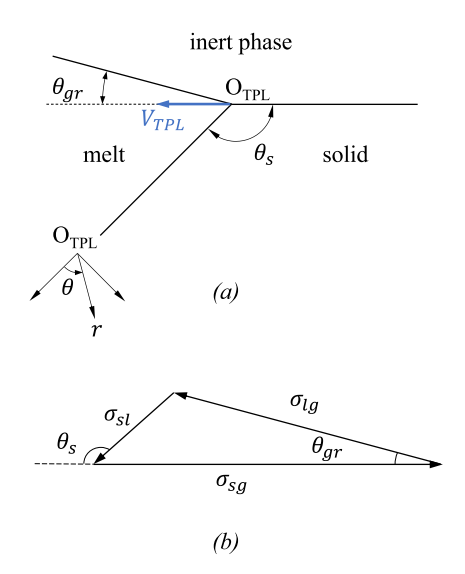


Fig. 1. (a) Schematic of the triple-phase line for an HRG-type configuration (b) corresponding equilibrium of interfacial tension vectors.

interface curvatures at the triple-phase line, it is difficult to know if the condition of minimum interfacial energies exists.

Furthermore, it is experimentally observed that when an advancing contact line approaches a sharp wedge, it gets pinned at the wedge corner and assumes a range of macroscopic contact angles before attaining a new equilibrium contact angle at the lower surface of the wedge (see e.g. section 1.2.1.2 in [1]). A similar pinning effect could occur at a triple-phase line causing the growth angle to assume a range of values at a triple-phase line.

In this paper, we provide an additional observation that the growth angle has an important effect on the behavior of the temperature field near the triple-phase line and conjecture that this sensitivity may influence the growth angles observed experimentally. The temperature field and thus the temperature gradients and heat fluxes at the triple-phase line are a function of the geometry defined by θ_{gr} and θ_{s} [7-10,12]. The relationship between the temperature and the triple-phase line geometry can be derived analytically from a local analysis near the triple-phase line as discussed in Section 2. Such analysis often leads to the identification of configurations of θ_s and θ_{gr} where the temperature gradients or heat fluxes become singular (i.e. approach infinity). The singularity of the temperature gradients at the triple-phase line can imply a breakdown of the continuum model or that important physics is missing from the model. It may also indicate configurations that are physically unlikely at the steady state. Therefore, the singularity analysis of the temperature field near the triple-phase line can indicate θ_s and θ_{gr} configurations that are nonsingular and therefore are more likely to be observed.

Anderson and Davis [7] performed such a singular point analysis assuming the solidification interface to be at the equilibrium melting temperature T_m with adiabatic conditions at the solid–gas and melt-gas interfaces. Helenbrook [8] extended their work by including non-zero heat fluxes at the interfaces. Pirnia and Helenbrook [9,10] added the effects of supercooling along the solid-melt interface but still modeled the inert phase as a heat flux. In our recent paper [12], we included the inert phase in the singular point analysis and obtained a general equation where the temperature near the triple-phase line can be determined as a function of thermal conductivities, solid and growth angles.

The purpose of this paper is to explore the relationship between the temperature field and the triple-phase line geometry as defined by θ_{gr} and θ_s . Conditions that lead to singular or nonsingular behavior are compared with geometries determined from interfacial tension balance and those observed experimentally.

2. Methods

In Fig. 1a a polar coordinate is defined with the initial ray $\theta = 0$ coincident with the solid-melt interface and positive angles measured counterclockwise. The solid, inert, and melt phases respectively correspond to $0 \le \theta \le \theta_s, \; \theta_s \le \theta \le \theta_{lg}, \; \text{and} \; \theta_{lg} \le \theta \le 2\pi \; \text{where}$ $\theta_{lg} = \theta_s + \pi - \theta_{gr}$. The subscripts s, l and g denote the solid, liquid, and inert phases. The subscript g is used for the inert phase since the inert phase is often a gas.

Near the triple-phase line shown in Fig. 1 the Peclet number, Pe_i = $\rho_i c_i V_{TPL} r/k_i \ll 1$ where the subscript $i \in \{g, l, s\}$ denotes the phase and ρ , c, and k represent density, specific heat at constant pressure, and thermal conductivity. Thus, as shown in [8,9], near the triple-phase line the steady-state energy equation reduces to Laplace's equation for temperature, T, as

$$\frac{1}{r}\frac{\partial}{\partial r}\left(r\frac{\partial T_i}{\partial r}\right) + \frac{1}{r^2}\frac{\partial^2 T_i}{\partial \theta^2} = 0. \tag{1}$$

Three boundary conditions stem from the temperature continuity along the interfaces

$$T_l(r, 2\pi) = T_s(r, 0),$$
 (2a)

$$T_{s}(r,\theta_{s}) = T_{\sigma}(r,\theta_{s}),$$
 (2b)

$$T_{g}(r,\theta_{lg}) = T_{l}(r,\theta_{lg}). \tag{2c}$$

Conservation of energy leads to three additional boundary conditions

$$-\frac{k_l}{r} \frac{\partial T_l}{\partial \theta} \bigg|_{\theta=2\pi} + \frac{k_s}{r} \frac{\partial T_s}{\partial \theta} \bigg|_{\theta=0} = -\rho_s L_f V_{TPL} \sin \theta_s, \tag{3a}$$

$$-\frac{k_{l}}{r}\frac{\partial T_{l}}{\partial \theta}\Big|_{\theta=2\pi} + \frac{k_{s}}{r}\frac{\partial T_{s}}{\partial \theta}\Big|_{\theta=0} = -\rho_{s}L_{f}V_{TPL}\sin\theta_{s}, \tag{3a}$$

$$-\frac{k_{s}}{r}\frac{\partial T_{s}}{\partial \theta}\Big|_{\theta=\theta_{s}} + \frac{k_{g}}{r}\frac{\partial T_{g}}{\partial \theta}\Big|_{\theta=\theta_{s}} = q_{rad,s}, \tag{3b}$$

$$-\frac{k_g}{r}\frac{\partial T_g}{\partial \theta}\bigg|_{\theta=\theta_{Ig}} + \frac{k_l}{r}\frac{\partial T_l}{\partial \theta}\bigg|_{\theta=\theta_{Ig}} = q_{rad,l},$$
(3c)

where L_f is the latent heat of fusion, and $q_{rad,i}$ with $i \in \{l, s\}$ is the net radiation heat flux from the melt and solid surfaces.

To determine the temperature, another boundary condition along a circle of finite radius about the triple-phase line is required, which is unknown. Still, using the known boundary conditions (2)a-(2)c and (3)a-(3)c, the behavior of the solution near the triple-phase line can be determined. The solution for this boundary value problem is derived in [12] as the sum of a homogeneous and a particular part. The particular solution is a linear function of r and can be written as $T_{i,p} = T_{TPL} + (A_i \cos(\theta) + B_i \sin(\theta)) r$ where T_{TPL} is the temperature at the triple-phase line and A_i and B_i are constants.

The homogeneous part of the solution can be written as

$$T_{i,h}(r,\theta) = \sum_{n=1}^{\infty} C_n \left(G_{i,n} \cos(\lambda_n \theta) + H_{i,n} \sin(\lambda_n \theta) \right) r^{\lambda_n}. \tag{4}$$

Each term in Eq. (4) is determined up to a scaling constant C_n where known coefficients $G_{i,n}$ and $H_{i,n}$ are components of eigenvectors corresponding to the eigenvalues $\lambda_n > 0$ which are determined from the numerical solution of

$$(1-a)\Big((a+b)(b-1)\cos\big(2\lambda(\theta_s-\theta_{gr})\big) - (b-a)(b+1)\cos\big(2\lambda(\pi-\theta_s)\big)\Big) - (1+a)\Big((b-a)(b-1)\cos(2\lambda\theta_{gr}) - (a+b)(b+1)\cos(2\lambda\pi)\Big) - 8ab = 0, (5)$$
where $a = \frac{k_s}{k_l}$ and $b = \frac{k_g}{k_l}$ [12].

3. Results and discussion

As discussed in Section 2, the temperature near the triple-phase line can be written as the sum of a linear particular solution and a homogeneous solution proportional to r^{λ_n} where $\lambda_n > 0$. The radial temperature gradients, and thus the heat fluxes, become singular at the triple-phase line if the dominant eigenvalue $\lambda_1 < 1$, which is obtained

Table 1
The material properties.

The material properties.							
Case	Materials	$T_m (K)^a$	$k_s \left(\frac{W}{mK}\right)$	$k_l \left(\frac{W}{mK} \right)$	$\frac{k_s}{k_l}$	$\frac{k_g}{k_l}$ b	
1	Si & Ar	1687	22 [23]	56 [24]	0.39	0.001	
2	Si & He	1687	22 [23]	56 [24]	0.39	0.010	
3	LiF & Ar	1121	5 [25]	1.3 [25]	3.8	0.048	
4	LiF & He	1121	5 [25]	1.3 [25]	3.8	0.396	
5	Al ₂ O ₃ c & Ar	2326	6.3 [26]	2.5 ^d	2.5 [15]	0.028	
6	Al ₂ O ₃ c & Ar	2326	6.3 [26]	4.2 ^d	1.5	0.017	
7	Al ₂ O ₃ c & Ar	2326	6.3 [26]	6.3 ^d	1 [16]	0.011	
8	Al ₂ O ₃ c & Ar	2326	6.3 [26]	9.4 ^d	0.67	0.008	
9	Ge & Ar	1211	17 [27]	37 [27]	0.46	0.010	
10	InSb & Ar	797	4.5 [28]	18 [29]	0.25	0.003	

- ^a From Ref. [30].
- $^{\rm b}~k_{\rm g}$ from Chapman–Enskog formula for monatomic gases at $T_{\rm m}$ [31].
- c Sapphire.
- d Based on assumed $\frac{k_s}{l}$.

from the numerical solution of Eq. (5). The singularity of the heat flux at the triple-phase line may indicate configurations that are physically unlikely at the steady state. To identify such configurations, defined by θ_{gr} and θ_s , the values of λ_1 were calculated from numerical solution of Eq. (5) on a two-dimensional θ_s - θ_{gr} grid with $0 < \theta_s < 180^\circ$ and $0 < \theta_{gr} < 90^\circ$ from which contour plots of $\lambda_1 - 1$ were obtained.

The dominant eigenvalue is a function of the thermal conductivities and solid and growth angles, $\lambda_1 = f(\frac{k_s}{k_l}, \frac{k_g}{k_l}, \theta_s, \theta_{gr})$. Thus, for a given pair of θ_s and θ_{gr} the value of λ_1 only depends on the ratios of thermal conductivities. Table 1 lists the thermal conductivities at the equilibrium melting temperature, T_m , for cases investigated. A comprehensive table of measured growth angles including the materials in Table 1 is given in [1]. Unfortunately, for most of the materials with measured growth angles, there is limited or no data on the thermal conductivities of the melt or solid at T_m . For instance, we could not find the thermal conductivity of the sapphire melt in literature. The value of \boldsymbol{k}_l for sapphire is often guessed by assuming a value for $\frac{k_s}{k_l}$ of 2.5 [15] or 1 [16]. Here, we used four assumed values of $\frac{2}{3} < \frac{k_s}{k_l} < 2.5$ for sapphire in cases 5–8 to demonstrate the effects of $\frac{k_s}{k_l}$ variations. Other materials with measured growth angles that appear to have no reported melt or solid thermal conductivities at T_m include $Y_3Al_5O_{12}$ ($\theta_{gr}=8^{\circ}$ [17]), LiNbO₃ ($\theta_{gr} = 4^{\circ}$ [18]), NaNO₃ ($\theta_{gr} = 2.5^{\circ}$ [19]), NaNO₂ ($\theta_{gr} = 7^{\circ}$ [20]), GaP ($\theta_{gr} = 10^{\circ}$ [21]), InP ($\theta_{gr} = 7^{\circ}$ [21]), and GaAs ($\theta_{gr} = 16$ [22]). Furthermore, in most of the cases where the growth angle is reported, the solid angle is also unknown.

The contours of $\lambda_1 - 1$ for solidifying silicon in contact with argon and helium are shown respectively in Figs. 2(a) and 2(b). The reported growth angle of 11° [32,33] is shown as a dashed line. Additionally, the values of solid angles observed in HRG experiments of [34,35] are shown in Figs. 2a-b with two markers. The details of each measured solid angle including the facet at the melt-solid interface and the pull direction are given in Table 2. Note that the growth angle was not measured in the HRG experiments and the growth angle from the literature does not report the solid angle. Interestingly, Fig. 2 indicates that when $\theta_s = 55^{\circ}$, the literature reported growth angle is close to the maximum value of λ_1 . The cross marker in Fig. 2 corresponds to a (111) facet with $\theta_s = 125^{\circ}$ that sometimes appears above the (111) facet with $\theta_s = 55^{\circ}$ creating a double facet at the leading edge of the silicon as shown in Fig. 2(c) [10,34]. The length of this (111) facet varies as the crystal grows and appears in some cross sections but not in others [34]. The facet angle of 125° at the triple-phase line leads to a singular temperature gradient, so thermally these two cases should be very different.

Considering the balance of interfacial tensions shown in Fig. 1(b) and assuming small curvatures for interfaces near the triple-phase line, equilibrium requires

$$\cos \theta_{gr} = \frac{\sigma_{sg}^2 + \sigma_{lg}^2 - \sigma_{sl}^2}{2\sigma_{sg}\sigma_{lg}},\tag{6a}$$

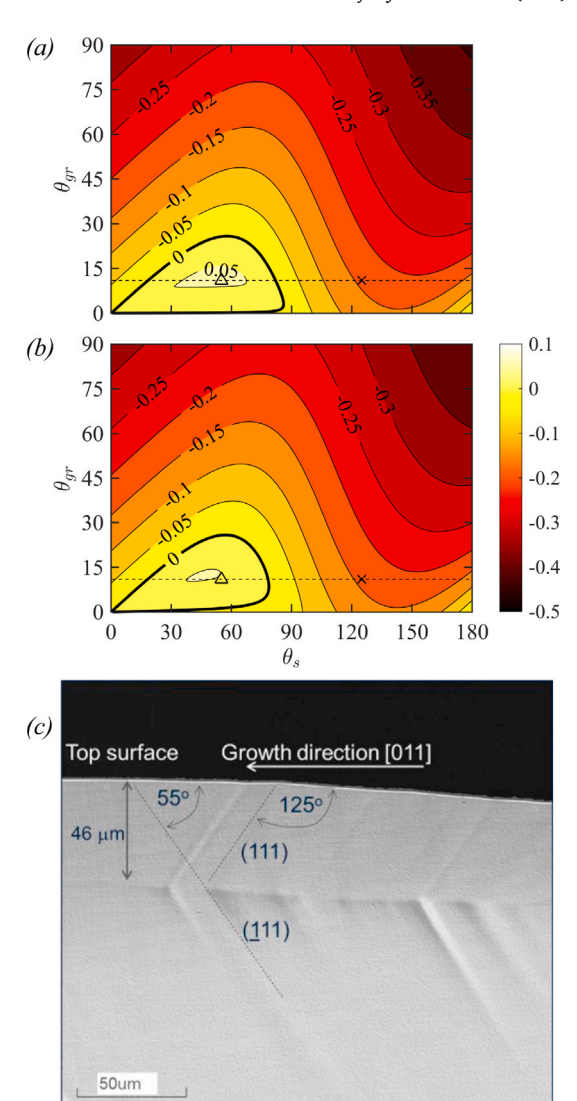


Fig. 2. Contours of $\lambda_1 - 1$ for (a) Si and Ar (b) Si and He (c) Double facet observed in HRG of silicon. The measured growth angle from [32] is shown with a dashed line. The Δ shows $\theta_3 = 55^\circ$. The \times shows $\theta_4 = 125^\circ$ for (111). (For interpretation of the references to color in this figure legend, the reader is referred to the web version of this article.)

Table 2
Solid angles observed for horizontal ribbon growth of silicon from [34,35].

θ_s	Facet ^a	Seed orientation ^b	Pull direction	Marker in Fig. 2
55°	(111)	(100)	[011]	Δ
125°	(111) ^c	(100)	[011]	×

- ^a The solid facet formed at the solid-melt interface near the triple-phase line.
- ^b The plane of the seed coincident with the top surface of the silicon ribbon.
- ^c Double facet; (111) facet was observed above a (111) facet.

$$\cos \theta_s = -\frac{\sigma_{sg}^2 + \sigma_{sl}^2 - \sigma_{lg}^2}{2\sigma_{sg}\sigma_{sl}}.$$
 (6b)

For solidification of a (111) facet of silicon, the interfacial energies from [36] are $\sigma_{sg}=1.05~\mathrm{J/m^2}$, $\sigma_{sl}=0.34~\mathrm{J/m^2}$, $\sigma_{lg}=0.83~\mathrm{J/m^2}$. These values result in $\theta_s=138^\circ$ and $\theta_{gr}=15^\circ$. This is somewhat consistent with the $\theta_s=125^\circ$ case but completely inconsistent with the $\theta_s=55^\circ$ case

Contours of λ_1 -1 for case 3 (LiF and argon with $\frac{k_g}{k_l} = 0.048$) and case 4 (LiF and helium with $\frac{k_g}{k_l} = 0.396$) are shown in Figs. 3(a) and 3(b)

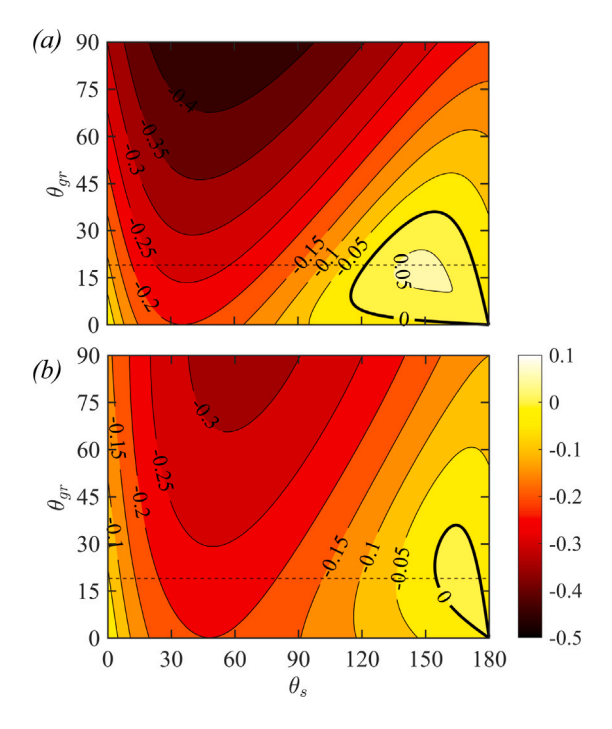


Fig. 3. The contours of $\lambda_1 - 1$ for (a) LiF and Ar (b) LiF and He. The dashed lines show the measured growth angle from [37]. (For interpretation of the references to color in this figure legend, the reader is referred to the web version of this article.)

Table 3
Measured growth angles for sapphire.

θ_{gr} (°)	Solid-melt interface	Reference
20 ± 5	Unknown	[40]
17 ± 4	Nonfaceted	[39]
35 ± 4	{0001} facet	[39]
12 ± 1	Unknown	[38]
12 ± 2	Unknown	[17]

respectively. Note that similar to Fig. 2, the experimentally reported growth angle from [37] passes through the points near the maximum of the nonsingular region in Figs. 3(a) and 3(b). Unfortunately, for LiF no solid angles were reported. Interfacial energies for LiF are also not known.

Fig. 4 shows the configurations with singular or nonsingular temperature gradients of sapphire where four different values were assumed for k_s/k_l to estimate k_l as given in Table 1 for cases 5 to 8. For $k_s = k_l$ (Fig. 4c) the only nonsingular growth angle is $\theta_{gr}=0$ and the λ_1 becomes independent of θ_s since the terms dependent on θ_s vanish in Eq. (5). Also, note that for $k_s < k_l$ and $k_s > k_l$ the nonsingular region corresponds to acute and obtuse solid angles respectively. The range of reported growth angles for sapphire as summarized in Table 3 is wider than other materials. The $\theta_{gr} = 12^{\circ}$ reported in two studies [17,38] passes through the maximum of the nonsingular region for $\frac{k_s}{k_s} = 2.5$ (as assumed in [15]). Using floating zone growth of sapphire, the growth angles of $\theta_{gr}=17^{\circ}$ and $\theta_{gr}=35^{\circ}$ were reported by Dreeben et al. [39] for non-faceted and {0001} facets at the solid-melt interface respectively. The solid angle is unknown as the orientation of the melt-solid interface was not reported. There again seems to be some correlation between the growth angle and the maximum in λ_1 , but again there is little data to make strong conclusions.

Figs. 5 and 6 respectively show the contours of λ_1-1 for solidification of germanium and Indium antimonide in contact with argon. There is some scatter within the measured growth angles but for all of them,

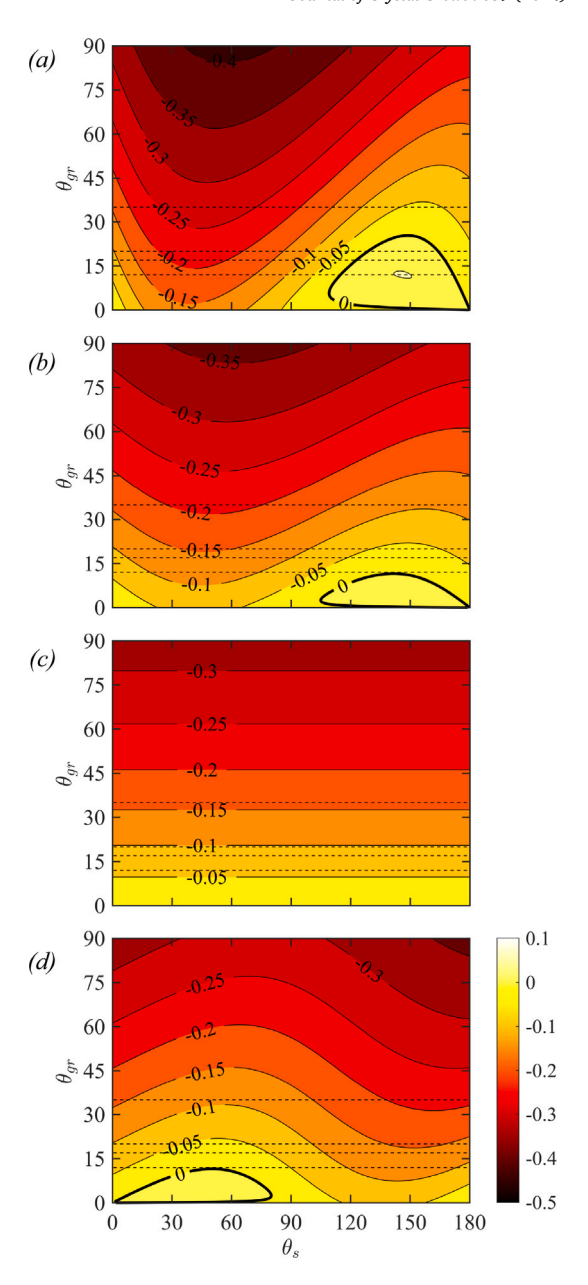


Fig. 4. Contours of $\lambda_1 - 1$ for single crystal Al_2O_3 (sapphire) and Ar assuming (a) $\frac{k_2}{k_1} = 2.5$ (b) $\frac{k_1}{k_1} = 1.5$ (c) $\frac{k_2}{k_1} = 1$ (d) $\frac{k_2}{k_1} = \frac{2}{3}$. Dashed lines show the measured growth angles from [17,38–40] (see Table 3). (For interpretation of the references to color in this figure legend, the reader is referred to the web version of this article.)

there is a range of solid angles with nonsingular heat fluxes. There is again no data on the solid angles that resulted in the measured growth angles. There is also no data on interfacial surface energies.

4. Conclusions

Observations were made on the correlation between observed growth angles and the growth angles that lead to nonsingular behavior at the triple-phase line. The singularity of the heat fluxes at the triple-phase line could imply various things such as a breakdown of the continuum assumption or incorrect or missing model physics. It could also indicate triple-phase line geometries that are physically unlikely at the steady state. For materials with experimentally measured growth angles, the reported data seems to fall in the range of conditions corresponding to where the heat fluxes are nonsingular. However, strong conclusions

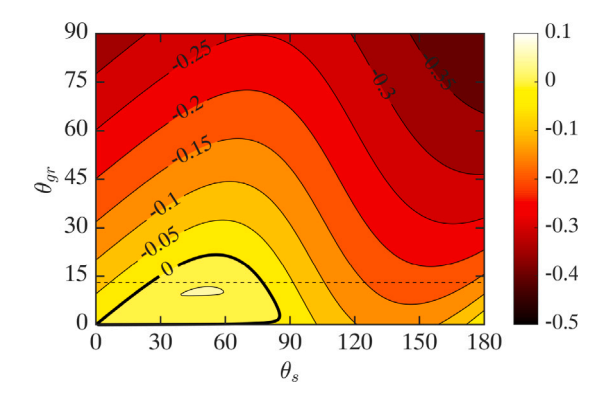


Fig. 5. Contours of $\lambda_1 - 1$ for single crystal Ge and Ar. The dashed line shows the measured growth angle from [41]. (For interpretation of the references to color in this figure legend, the reader is referred to the web version of this article.)

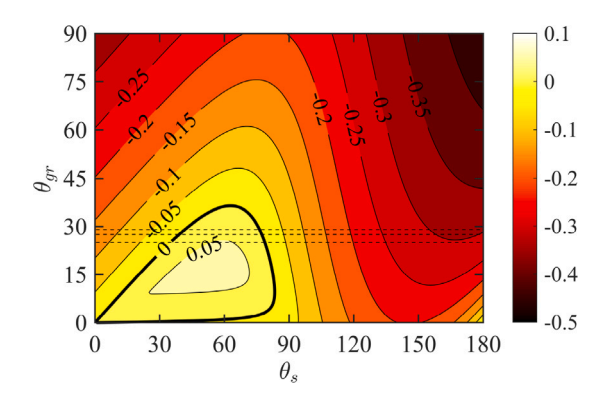


Fig. 6. Contours of λ_1-1 for single crystal InSb and Ar. The dashed line shows the measured growth angle from [22,38,42]. (For interpretation of the references to color in this figure legend, the reader is referred to the web version of this article.)

cannot be made because of the limited data available on growth angle, solid angle, and thermal conductivities.

Similarly, it was hard to draw conclusions about whether an interfacial tension balance exists at the triple-phase line because of the lack of data on interfacial energies. Further experimental work or possibly molecular dynamic simulations are needed to draw any conclusions about whether either of these criteria is predictive of the observed growth angles.

CRediT authorship contribution statement

Nojan Bagheri-Sadeghi: Writing – original draft, Visualization, Methodology, Investigation, Formal analysis, Conceptualization. **Brian T. Helenbrook:** Writing – review & editing, Supervision, Resources, Project administration, Funding acquisition, Conceptualization.

Declaration of competing interest

The authors declare that they have no known competing financial interests or personal relationships that could have appeared to influence the work reported in this paper.

Data availability

No data was used for the research described in the article.

Acknowledgments

This material is based upon work supported by the National Science Foundation, United States under Grant Nos. 1762802 and 2317674.

References

- [1] N. Eustathopoulos, B. Drevet, S. Brandon, A. Virozub, Basic principles of capillarity in relation to crystal growth, in: T. Duffar (Ed.), Crystal Growth Processes Based on Capillarity, John Wiley & Sons, 2010, pp. 1–49, http: //dx.doi.org/10.1002/9781444320237.ch1, Ch. 1.
- N. Van den Bogaert, F. Dupret, Simulation of back-melting in Czochralski growth,
 J. Cryst. Growth 166 (1) (1996) 446–451, http://dx.doi.org/10.1016/0022-0248(96)00135-2.
- [3] N. Bagheri-Sadeghi, B.T. Helenbrook, Buoyancy and Marangoni effects on horizontal ribbon growth, J. Cryst. Growth 596 (2022) 126822, http://dx.doi.org/10.1016/j.jcrysgro.2022.126822.
- [4] W. Bardsley, F. Frank, G. Green, D. Hurle, The meniscus in Czochralski growth, J. Cryst. Growth 23 (4) (1974) 341–344, http://dx.doi.org/10.1016/0022-0248(74) 90081-5.
- [5] T. Surek, S. Coriell, B. Chalmers, The growth of shaped crystals from the melt, J. Cryst. Growth 50 (1) (1980) 21–32, http://dx.doi.org/10.1016/0022-0248(80)90227-4.
- [6] R.A. Brown, Theory of transport processes in single crystal growth from the melt, AIChE J. 34 (6) (1988) 881–911, http://dx.doi.org/10.1002/aic.690340602.
- [7] D. Anderson, S. Davis, Fluid flow, heat transfer, and solidification near trijunctions, J. Cryst. Growth 142 (1) (1994) 245–252, http://dx.doi.org/10.1016/ 0022-0248(94)90293-3.
- [8] B.T. Helenbrook, Solidification along a wall or free surface with heat removal,
 J. Cryst. Growth 418 (2015) 79–85, http://dx.doi.org/10.1016/j.jcrysgro.2015.
 02.028.
- [9] A. Pirnia, B.T. Helenbrook, Analysis of faceted solidification in the horizontal ribbon growth crystallization process, J. Cryst. Growth 555 (2021) 125958, http://dx.doi.org/10.1016/j.jcrysgro.2020.125958.
- [10] A. Pirnia, B.T. Helenbrook, Physics of double faceted crystal growth in solidification processes, J. Crystal Growth 582 (2022) 126517, http://dx.doi.org/10.1016/j.jcrysgro.2022.126517.
- [11] N. Bagheri-Sadeghi, V.A. Fabiyi, B.T. Helenbrook, E. Paek, Sensitivity of horizontal ribbon growth to solidification kinetics, J. Cryst. Growth 603 (2023) 127038, http://dx.doi.org/10.1016/j.jcrysgro.2022.127038.
- [12] N. Bagheri-Sadeghi, B.T. Helenbrook, Effects of the inert phase on solidification near a triple-phase line, J. Cryst. Growth 625 (2024) 127438, http://dx.doi.org/ 10.1016/j.jcrysgro.2023.127438.
- [13] N. Bagheri-Sadeghi, B.T. Helenbrook, Gas effects on horizontal ribbon growth, J. Cryst. Growth 634 (2024) 127675, http://dx.doi.org/10.1016/j.jcrysgro.2024. 127675.
- [14] V. Voronkov, Theory of crystal surface formation in the pulling process, J. Cryst. Growth 52 (1981) 311–318, http://dx.doi.org/10.1016/0022-0248(81)90210-4.
- [15] G. Samanta, A. Yeckel, P. Daggolu, H. Fang, E.D. Bourret-Courchesne, J.J. Derby, Analysis of limits for sapphire growth in a micro-pulling-down system, J. Cryst. Growth 335 (1) (2011) 148–159, http://dx.doi.org/10.1016/j.jcrysgro.2011.09. 015
- [16] N. Zhang, H.G. Park, J.J. Derby, Simulation of heat transfer and convection during sapphire crystal growth in a modified heat exchanger method, J. Cryst. Growth 367 (2013) 27–34, http://dx.doi.org/10.1016/j.jcrysgro.2013.01.011.
- [17] M.M. Fejer, J.L. Nightingale, G.A. Magel, R.L. Byer, Laser-heated miniature pedestal growth apparatus for single-crystal optical fibers, Rev. Sci. Instrum. 55 (11) (1984) 1791–1796, http://dx.doi.org/10.1063/1.1137661.
- [18] R. Feigelson, Pulling optical fibers, J. Cryst. Growth 79 (1, Part 2) (1986) 669–680, http://dx.doi.org/10.1016/0022-0248(86)90535-X.
- [19] C. Lan, S. Kou, Heat transfer, fluid flow and interface shapes in floating-zone crystal growth, J. Cryst. Growth 108 (1) (1991) 351–366, http://dx.doi.org/10. 1016/0022-0248(91)90383-G.
- [20] L. Kuandykov, P. Antonov, Shaped melt column optimal choice on the basis of an equilibrium growth angle value, J. Cryst. Growth 222 (4) (2001) 852–861, http://dx.doi.org/10.1016/S0022-0248(00)01010-1.
- [21] V. Antonov, V. Selin, The growth angle and particular case of stabilization of the shape of the crystallized small drops of the melt, J. Cryst. Growth 241 (4) (2002) 507–511, http://dx.doi.org/10.1016/S0022-0248(02)01286-1.
- [22] G. Satunkin, Determination of growth angles, wetting angles, interfacial tensions and capillary constant values of melts, J. Cryst. Growth 255 (1) (2003) 170–189, http://dx.doi.org/10.1016/S0022-0248(03)01187-4.
- [23] M. Mito, T. Tsukada, M. Hozawa, C. Yokoyama, Y.-R. Li, N. Imaishi, Sensitivity analyses of the thermophysical properties of silicon melt and crystal, Meas. Sci. Technol. 16 (2) (2005) 457–466, http://dx.doi.org/10.1088/0957-0233/16/2/ 018.
- [24] H. Kobatake, H. Fukuyama, T. Tsukada, S. Awaji, x, Meas. Sci. Technol. 21 (2) (2010) 025901, http://dx.doi.org/10.1088/0957-0233/21/2/025901.

- [25] D.A. Jaworske, W.D. Perry, Hot Filament Technique for Measuring the Thermal Conductivity of Molten Lithium Fluoride, Tech. Rep. 102506, 1990, URL https: //ntrs.nasa.gov/citations/19900010057.
- [26] A.M. Hofmeister, Thermal diffusivity and thermal conductivity of single-crystal MgO and Al_2O_3 and related compounds as a function of temperature, Phys. Chem. Min. 41 (5) (2014) 361–371, http://dx.doi.org/10.1007/s00269-014-0655-3
- [27] V. Golyshev, M. Gonik, V. Tsvetovsky, Study of thermal conductivity close to the melting point, High Temp. - High Press. 35 (2) (2003) 139–148.
- [28] S. Nakamura, T. Hibiya, F. Yamamoto, Thermal conductivity of GaSb and InSb in solid and liquid states, J. Appl. Phys. 68 (10) (1990) 5125–5127, http://dx.doi.org/10.1063/1.347051.
- [29] S. Nakamura, T. Hibiya, Thermophysical properties data on molten semiconductors, Int. J. Thermophys. 13 (6) (1992) 1061–1084, http://dx.doi.org/10.1007/BF01141216.
- [30] W.M. Haynes (Ed.), CRC Handbook of Chemistry and Physics, 97th ed., CRC Press, 2016, http://dx.doi.org/10.1201/9781315380476.
- [31] R. Bird, W. Stewart, E. Lightfoot, Transport Phenomena, second ed., Wiley, 2002.
- [32] T. Surek, B. Chalmers, The direction of growth of the surface of a crystal in contact with its melt, J. Cryst. Growth 29 (1) (1975) 1–11, http://dx.doi.org/ 10.1016/0022-0248(75)90041-X.
- [33] M. Hamidi, H. Rodot, Méthode de détermination de l'angle de croissance d'un matériau : Application au silicium, Rev. Phys. Appl. 18 (2) (1983) 75–80, http://dx.doi.org/10.1051/rphysap:0198300180207500.
- [34] P. Kellerman, B. Kernan, B.T. Helenbrook, D. Sun, F. Sinclair, F. Carlson, Floating silicon method single crystal ribbon – observations and proposed limit cycle theory, J. Cryst. Growth 451 (2016) 174–180, http://dx.doi.org/10.1016/ j.jcrysgro.2016.07.012.

- [35] P. Daggolu, J. Appel, P. Kellerman, N. Stoddard, Pulling thin single crystal silicon wafers from a melt: The new leading-edge solar substrate, J. Cryst. Growth 584 (2022) 126561, http://dx.doi.org/10.1016/j.jcrysgro.2022.126561.
- [36] G. Barinovs, A. Sabanskis, A. Muiznieks, Study of silicon crystal surface formation based on molecular dynamics simulation results, J. Cryst. Growth 391 (2014) 13–17, http://dx.doi.org/10.1016/j.jcrysgro.2014.01.004.
- [37] P. Antonov, V. Krymov, E. Hartmann, Growth and properties of shaped single crystals of lithium fluoride, J. Cryst. Growth 104 (1) (1990) 142–147, http://dx.doi.org/10.1016/0022-0248(90)90323-D.
- [38] G. Satunkin, V. Tatarchenko, V. Shaitanov, Determination of the growth angle from the shape of a crystal lateral face and solidified separation drops, J. Cryst. Growth 50 (1) (1980) 133–139, http://dx.doi.org/10.1016/0022-0248(80) 90238-9.
- [39] A. Dreeben, K. Kim, A. Schujko, Measurement of meniscus angle in laser heated float zone growth of constant diameter sapphire crystals, J. Cryst. Growth 50 (1) (1980) 126–132, http://dx.doi.org/10.1016/0022-0248(80)90237-7.
- [40] V. Tatarchenko, G. Satunkin, Capillary shaping in crystal growth from melts: II. Experimental results for sapphire, J. Cryst. Growth 37 (3) (1977) 285–288, http://dx.doi.org/10.1016/0022-0248(77)90121-X.
- [41] T. Surek, The meniscus angle in germanium crystal growth from the melt, Scr. Metall. 10 (5) (1976) 425–431, http://dx.doi.org/10.1016/0036-9748(76)90166-
- [42] H. Rodot, M. Hamidi, J. Bourneix, A. Okhotin, I. Zoubridski, V. Kriapov, E. Markov, Crystal growth method under microgravity conditions, J. Cryst. Growth 52 (1981) 478–484, http://dx.doi.org/10.1016/0022-0248(81)90237-2.